PCCP
Physical Chemistry Chemical Physics

Accepted Manuscript

This article can be cited before page numbers have been issued, to do this please use: D. S. Bertoldi, E. N. Millán and A. Fernández Guillermet, *Phys. Chem. Chem. Phys.*, 2020, DOI: 10.1039/D0CP04442C.

ROYAL SOCIETY OF CHEMISTRY

rsc.li/pccp

View Article Online
DOI: 10.1039/D0CP04442C

PCCP

ARTICLE TYPE

Cite this: DOI: 00.0000/xxxxxxxxxx

Phenomenology of the heating, melting and diffusion processes in Au nanoparticles †

Dalía S. Bertoldi,*[a] Emmanuel N. Millán,[b] and A. Fernández Guillermet[c]

Received Date
Accepted Date

DOI: 00.0000/xxxxxxxxxx

The paper reports the results of a Molecular Dynamics study of the heating and melting process of nanoparticles with 1985 to 84703 atoms. Building on a previous study by the present authors [Bertoldi et al. Journal of Physics and Chemistry of Solids, 2017, 111, pp. 286-293] involving the energy versus temperature, the Lindemann index and the radial distribution function, the current work relies on the mean-square displacement, the Lindemann ratio and the simulated snapshots to characterize four regions in the process of heating-to-melting. A general pattern of the atomic configuration evolution upon heating and a systematics of the transition temperatures between the various identified steps, is proposed. In addition, the most significant, so-called "melting step" in this process is analyzed in terms of the quasi-chemical approach proposed by Bertoldi et al., which treats this step by invoking a dynamic equilibrium of the type Au (LEA-SPL) $\rightleftharpoons$ Au (HEA-LPL) involving low-energy atoms (LEA) and high-energy atoms (HEA) forming the solid phase-like (SPL) and the liquid phase-like (LPL) states of the system, respectively. The "melting step" is characterized by evaluating the equal-Gibbs energy temperature, i.e., the "T_0 temperature", previously introduced by the current authors, which is the thermodynamic counterpart of the temperature of fusion of macroscopic elemental solids. The diffusion coefficients at T_0 are determined, and their spatial and temperature dependence is discussed. In particular, the activation energy for the atom movements in the HEA-LPL/LEA-SPL mixture at T_0 is reported. The consistency between the current phenomenological picture and microscopic interpretation of the thermodynamic, kinetic and atomic configuration information obtained is highlighted.

1 Introduction

The effect of temperature upon the atomic configuration, the thermodynamic and kinetic properties of nanoparticles has been a subject of considerable research attention in the last three decades[1–17]. In this field, Molecular Dynamics (MD) simulations have traditionally been used as a valuable tool to determine the thermodynamic evolution of the nanoparticles upon heating[5,6,12–14,17]. A key result of the thermodynamically focused MD work on elements is the fact that at sufficiently high temperatures, solid "phase-like" structures coexist with liquid "phase-like" structures in a temperature range, contradicting what is expected from Gibbs' Rule for the coexistence of phases in macroscopic materials, viz., a unique melting temperature. These features were early conceptualized by Berry and collaborators[3,10,18,19] and other authors (e.g., by Honeycutt and Andersen[20]) by invoking the concept of a dynamical equilibrium between the atoms in the solid phase-like and the liquid phase-like parts of the system. In this qualitative picture, the melting transition is treated as an increase with temperature of the relative amounts of the atoms in the liquid phase-like parts of the system. In a recent work, the current authors[21] used MD simulations to characterize thermodynamically the heating and melting process of spherical Au nanoparticles. To this end, MD simulations were used to establish the energy-versus-temperature, so-called "caloric curves", as well as to describe the configuration of the phase-like parts, such as the Lindemann index and the radial distribution function[21]. On these bases, a tentative thermodynamic model of the melting transition in Au was developed. In particular, in the temperature range where most of the melting process occurs, referred to as the "melting step", the system was found in the simulated snapshots to consist of a mixture of two kinds of atoms, viz., the low-energy atoms (LEA) forming the solid phase-like (SPL), and high-energy atoms (HEA) forming the liquid phase-like (LPL)[21]. In addition, the calculated snapshots as a function of temperature indicated that the mixture of LEA and HEA in the melting step was in principle consistent with the qualitative picture of a dynamical equilibrium developed by Berry and others. This qualitative agreement encouraged a quantitative treatment of the melting step, by treating the dynamical equilibrium between the

[a] Facultad de Ingeniería, Universidad Nacional de Cuyo, Mendoza, Argentina, E-mail: daliasurena_ber@hotmail.com
[b] CONICET and ITIC, Universidad Nacional de Cuyo, Mendoza, Argentina.
[c] CONICET - Instituto Balseiro, Centro Atómico Bariloche, Argentina.

View Article Online
DOI: 10.1039/D0CP04442C

LEA and HEA in terms of a classical physico-chemical formalism applicable to a isomerization-type reaction, viz., Au (LEA-SPL) $\rightleftharpoons$ Au (HEA-LPL) . In particular, the equilibrium constant was introduced, and the involved atomic fractions of HEA-LPL and LEA-SPL in the mixture were evaluated from the energy boundaries of the melting step in the caloric curve[21]. Encouraged by the results of such an analysis, in the present work we aim at going on one step further, by studying the changes in the atomic configurations, the kinetic properties and other implications of the previously introduced quasi-chemical picture and concepts. Specifically, the current work focuses both on the phenomenology and the microscopic details of the heating and the SPL-to-LPL change, with particular attention to the role of diffusion. To this end, MD simulations are used to evaluate the Lindemann ratio[22–24], i.e., a parameter that is sensitive to the changes in the atomic configuration and can be directly related to the diffusion coefficients. On these bases, a picture of the effects of heating and melting upon the atomic configuration, thermodynamic and kinetic properties of the nanoparticles is presented. In particular, a discussion of the activation energy for diffusion in the range of the dynamic coexistence between the LEA-SPL and the HEA-LPL, is reported.

2 Computational Methodology

2.1 Simulations details

A set of 13 gold nanoparticles with a number of atoms (N) ranging from 1985 to 84703 were created with the LAMMPS code[25], as spheres of different radius centered at the origin of the fcc lattice. An EAM interaction potential[26] extensively used to study the melting of Au nanoparticles[4,27–30] was adopted. The current nanoparticles have a free-surface boundary condition at given temperatures under zero external pressure. The temperature (T) was increased as follows: for heating up to 800 K a heating rate of 0.1 K/ps was adopted, but above that the rate was reduced to 0.02 K/ps until the melting occurred. At each temperature, a MD run of 500 ps was made: the first 400 ps were used for equilibration and the following 100 ps to obtain statistical data.

Finally, in order to start with the most stable configuration, an energy minimization procedure was applied at the beginning of the MD runs. A similar treatment of the heating process has been used in previous works[5,21,30].

2.2 Exploratory runs

As a part of the work, two sets of exploratory runs were performed, involving the nanoparticle of N =15707. The first set was aimed at determining the effect of changes in the heating rate upon the observed temperature boundaries of the melting step. To this purpose, various rates were tested in the range of most importance for the study of the temperatures of the heating-to-melting process, viz., for $T > 800$ K. All tested runs adopted a heating rate of 0.1 K/ps up to 800 K, but at higher temperatures, the following alternative rates were tested: (i) 0.01 K/ps; (ii) 0.05 K/ps; and (iii) 0.1 K/ps. The resulting mean-square displacement (MSD) versus temperature curves, are compared in Fig. 1 (a) with the curve corresponding to the heating rate used in the present work to determine the characteristic temperatures above

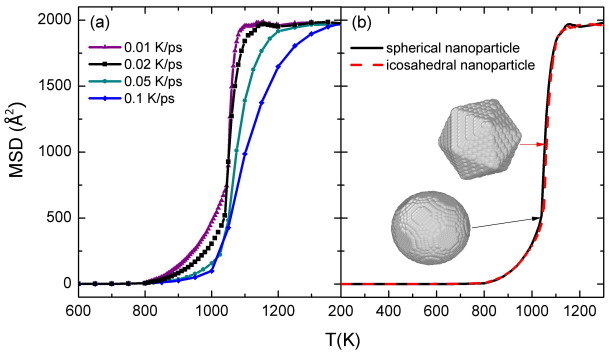

Fig. 1 The MD simulated temperature dependence of the mean-square displacement (MSD) for nanoparticles with and 15707 atoms as a function of temperature, determined in the current exploratory runs, described in Sect.2.2.. The (a) panel compares the results obtained by changing the heating rates. The (b) panel compares the results corresponding to spherical nanoparticles with those for icosahedral nanoparticles with a similar number of atoms.

800 K, viz., 0.02 K/ps. Figure 1 (a) indicates that the current combination yields a MSD vs. temperature line differing very little from lowest rates tested, viz., the combination 0.1 K/ps up to 800K followed by 0.01 K/ps. In view of this fact, current combination (i.e., 0.1 K/ps up to 800 K followed by 0.02K/ps up to the melting range) was accepted, by considering it as a reasonably good compromise of accuracy and computer time.

The second set of exploratory runs was aimed at testing the effect upon the MSD vs. T curve of changing the shape of the N =15707 nanoparticle. To this aim the results corresponding to spherical nanoparticles are compared in Fig. 1 (b) with those for icosahedral ones with $N = 15512$, i.e., with a similar number of atoms. The icosahedral nanoparticles were generated using nanoSCULPT[31]. The MSD vs. T lines compared in Fig. 1 (b) are close enough to tentatively hypothesize that the characteristic temperatures for the heating-and-melting process determined in Sect.3.1 using extensive results for spherical nanoparticles, might be representative of the behavior of other shapes. In order to fully test this hypothesis, i.e., by including the thermodynamic and kinetic properties discussed in the present paper, a new research project, complementary of the current work, has been initiated and the results will be presented in a forthcoming paper.

2.3 Cohesive energy

Before increasing the temperature, the energy values at $T = 0$ K were determined, and used to calculate the energy difference between each nanoparticle (hereafter denoted by "np") and macroscopic ("m") Au. To this aim a single simulation of macroscopic Au was performed at that temperature using 20x20x20 cells and periodic boundary conditions. The so-obtained energy value per atom, viz., -3.93eV, coincides with that obtained in ref.[30] using the same potential. With this new information, the cohesive energy difference $\Delta E_{\rm coh} = {E_{\rm coh}}^{m} - {E_{\rm coh}}^{np}$ was evaluated, and also included in the discussion of the melting process (see Fig. 6 in Sect. 4.2).

View Article Online
DOI: 10.1039/D0CP04442C

2.4 Mean-square displacement and the Lindemann ratio

The MD results were used to study the variation with temperature of the quantity δ_L connecting the MSD of the atoms with the nearest-neighbor distance (χ), viz.,

$$(\delta_L \chi)^2 = \text{MSD} \quad (1)$$

δ_L is usually known as the Lindemann ratio, because it is involved in the oldest empirical picture of the melting phenomenon in macroscopic solids, i.e., the Lindemann criterion[32]. In order to apply Eq.(1), the MSD was evaluated as the deviation of the position of each atom from a reference, initial position:

$$\text{MSD} = \langle (r_i(t) - r_i(0))^2 \rangle \quad (2)$$

where <...> denotes the atomic average, $r_i(0)$ is the reference position and $r_i(t)$ the corresponding position at the time t. We emphasize that other definitions of the MSD are found in the literature (see, e.g., ref.[33]). In the current calculations, the average nearest-neighbor distance χ was estimated from the MD calculated average volume (V) per atom (V/N) by using the following relation:

$$\left(\frac{(V/N)^{np}(T)}{(V/N)^{m}(0)} \right)^{1/3} = \frac{\chi^{np}(T)}{\chi^{m}(0)} \quad (3)$$

Taking into account that macroscopic Au at atmospheric pressure is stable in the fcc structure, Eq.(3) yields

$$\chi^{np}(T) = \frac{\sqrt{2}}{2} [4(V/N)^{np}(T)]^{1/3} \quad (4)$$

A similar relationship between V/N and χ has previously been adopted[24] to treat a Lennard-Jones fcc nanocrystal.

2.5 Diffusion coefficients

The diffusion coefficient (D) was calculated for each temperature from the slopes of the linearized MSD versus time (t) relations, using the Einstein equation[6,12,33]:

$$D = \frac{1}{6} \frac{(\delta_L \chi)^2}{t} \quad (5)$$

Taking into account that there are references where it is reported that in finite nanoparticles MSD "saturates" at large t[6,33], the slopes were determined by considering a time interval t=500 ps, i.e., before such "saturation" phenomenon occurs. The chosen time interval is also long enough to allow the fluctuations to average.

3 Results

3.1 Systematics of the δ_L versus T relations

In a previous work, a picture of the effects of heating and melting upon the atomic configuration of nanoparticles was developed, which involved various characteristic temperatures ranges. The temperature boundaries of these ranges were determined from plots of the MD results by analyzing the rate of change with temperature of the energy and the Lindemann index, combined with the relevant snapshots and taking into account the information provided by other properties, viz., the root-mean square displacement and the radial distribution function[21]. In the present subsection, the boundaries of the previously identified temperature ranges, as well as the details of the atomic configuration changes upon heating will be further studied by analyzing plots of the Lindemann parameter (δ_L) as a function of T combined with MD produced snapshots at various selected temperatures.

The δ_L vs. T curves corresponding to 6 of the 13 nanoparticles with $1985 \leq N \leq 84703$ are presented in Fig. 2. The curves present the same general characteristics. The most significant one is a drastic increase in δ_L occurring in a temperature range whose boundaries are denoted by T_2 and T_3 (see below). These temperatures depend of N, being lower for the small nanoparticles, i.e., those with the largest surface-to-volume ratio. This feature, and the type of size dependence shown by other relevant temperatures, reflects the fact that atoms on the surface have weaker restraining forces than the inner atoms. Consequently, the average cohesive energy per atom of the smaller nanoparticles is lower than that of the larger ones, i.e., the MD calculated ΔE_{coh} quantity increases with decreasing N (see Fig. 6 in Sect. 4.2).

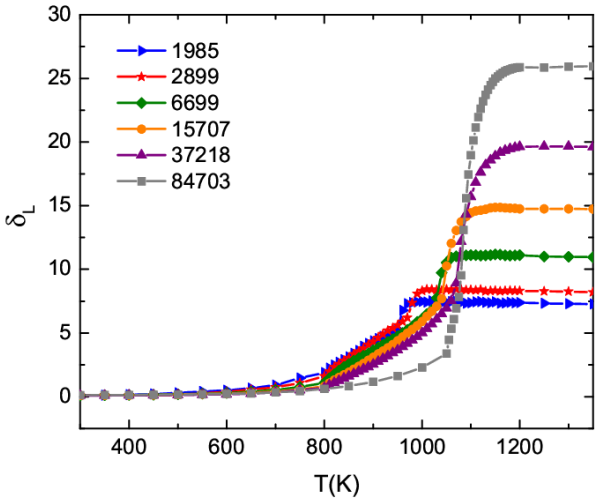

Fig. 2 The Lindemann ratio (δ_L) versus temperature (T) values for nanoparticles with 1985 to 84703 atoms (symbols). The lines are only guides to the eye.

Four characteristic temperatures referred to as T^*, T_1, T_2 and T_3 were determined, and used to construct dimensionless δ_L versus T/T_3 plots such as those presented in Fig. 3 for 6 of the 13 nanoparticles with $1985 \leq N \leq 15707$.

In Fig. 3 we also include MD simulated snapshots. The atoms located in the surface at the onset of the heating process are painted in red. The vertical dotted lines indicate the ratios between various characteristic temperatures and T_3. This information will be interpreted in terms of the atomic process taking place in regions I to IV, indicated by the roman numbers in Fig. 3, as follows.

In Region I the material is found in the SPL state. In this temperature range, two sub-regions are distinguished: one characterized by a linear (Sect. 3.2) and the other by a non-linear variation

View Article Online
DOI: 10.1039/D0CP04442C

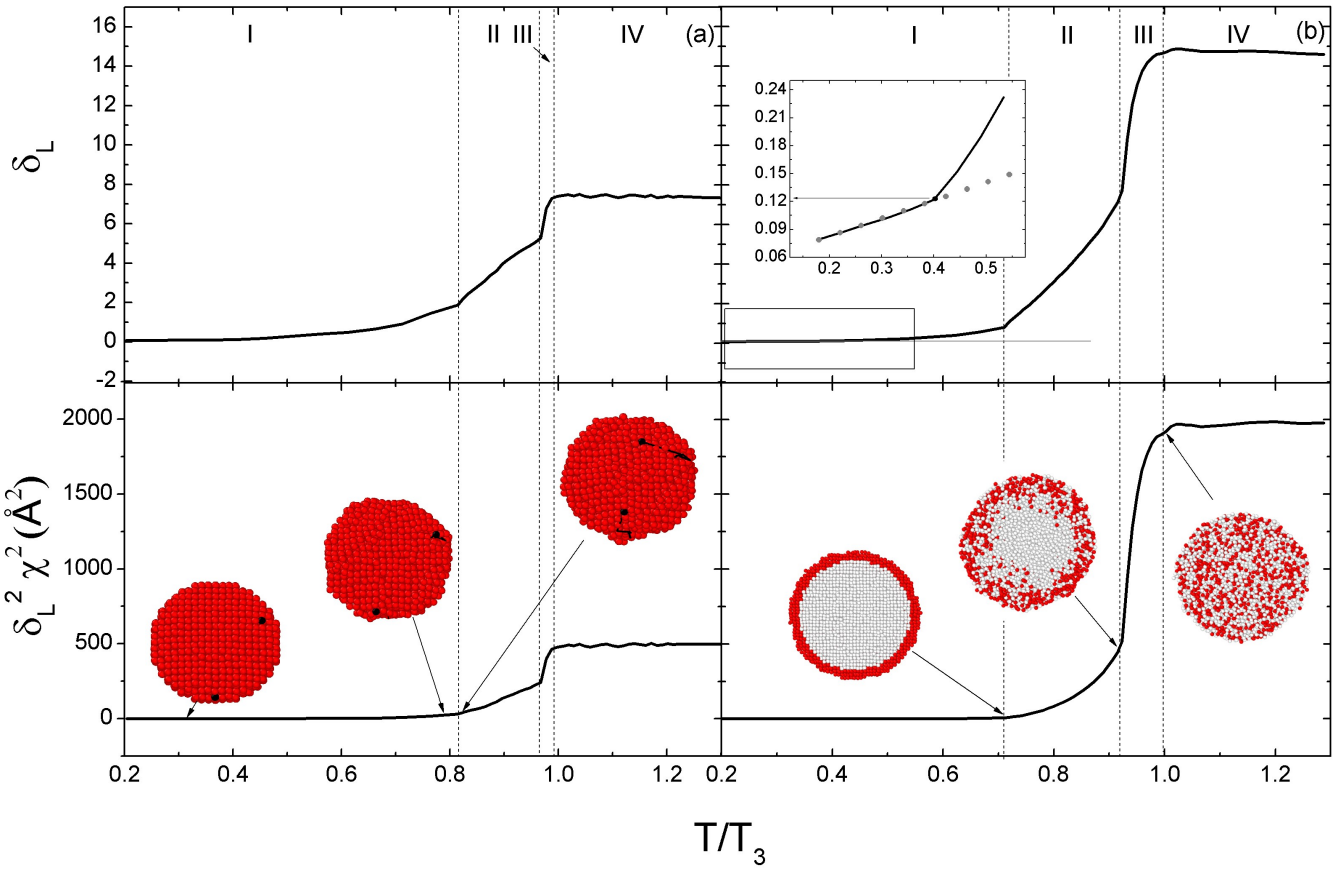

Fig. 3 The MD simulated temperature dependence of the Lindemann ratio (δ_L) and the MSD ($(\delta_L X)^2$) for nanoparticles with 1985 ((a) panels) and 15707 atoms ((b) panels) as a function of the dimensionless T/T_3 ratio. The vertical dotted lines indicate the boundaries of the four regions (I to IV) distinguished in the heating and melting process.The inset in the (b) panel shows the linear MSD vs. T region. In the snapshots the Au atoms located in the surface at the onset of the heating process are painted in red, and the inner atoms are painted in gray. In the snapshot in Fig.3(a) the diffusion on the surface is indicated by marking in black the displacement of two such atoms.

of δ_L with temperature. Region I ends at temperatures T_1, where a significant increase in the rate of change of the MSD (and δ_L) with temperature is observed. This has been interpreted as the beginning of the "pre-melting"[21], indicated as region II. For the present nanoparticles it is found that $0.8 \geq T_1/T_3 \geq 0.6$.

In Region II the atoms on the surface of the nanoparticles start to diffuse. This is shown by the snapshots in 3(a), where we have marked in black the displacement of two such atoms. At temperatures higher than T_1 (see below), the surface atoms diffuse towards the center of the nanoparticle, so that the T_1/T_3 ratio will be taken as a measure of the temperatures where volume diffusion processes are noticeable in the current nanoparticles. The consequences of this assumption will be examined at the end of the present section, by referring to Fig. 4.

Region II ends at the temperature T_2 where an even more rapid increase of δ_L (and the MSD) with temperature occurs. This is interpreted as the start of the "melting step", indicated as Region III. The MD simulated snapshots in 3(b), corresponding to a section through the center of the nanoparticle, indicate that the diffusion that started at the surface reaches the inner atoms, with the atoms painted in red and in gray coexisting in a mixture with comparable proportions. This feature, clearly seen in the snapshots in 3(b) as well as in those reported in Fig.2 of our previous work[21], is compatible with the assumption that the melting step involves a proper mixture of two kinds of atoms, which is adopted by the quasi-chemical model formulated in Sect. 4.1. For the current nanoparticles it is found that $0.97 \geq T_2/T_3 \geq 0.90$. In Sect. 4.3 the kinetic properties of this region will be studied by focusing on a specific, thermodynamically relevant temperature T_0, such that $T_2 < T_0 < T_3$.

In Region IV, corresponding to $T/T_3 > 1$, the nanoparticles are found in the LPL state. The δ_L vs. T (and the MSD vs. T) relation reaches a plateau, indicating that the atoms diffuse through the whole nanoparticle. The section snapshots (Fig.3(b)) show a full mixture of the atoms painted in red and in gray. In addition, the δ_L and MSD values corresponding to the plateaus increase with N. Taken into account that the MSD values are principally (but not only, see below) spatial dependent, this trend is interpreted as indicating that the larger nanoparticles in the LPL state offer more room for the atoms to move. The spatial dependence together with the temperature dependence of the MSD will be further considered in Sect.4.3 when analyzing the systematics of diffusion

View Article Online
DOI: 10.1039/D0CP04442C

coefficients determined within the melting step (Fig. 7).

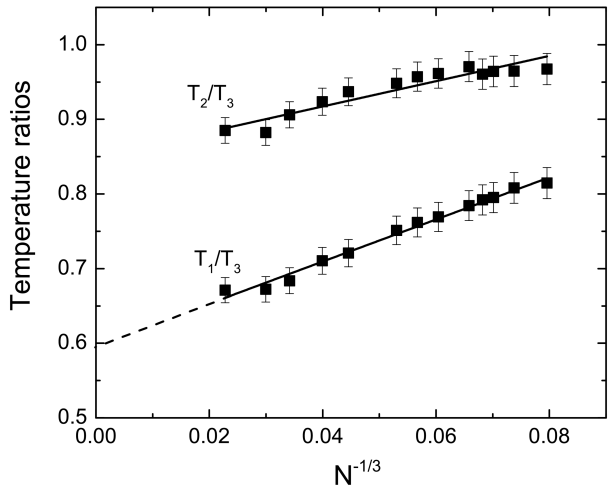

Fig. 4 The size dependence of the dimensionless ratios T_1/T_3 and T_2/T_3 involving the temperature boundaries of regions I to III (see text). The solid squares with error bars represent the ratios determined in Sect. 3 from the MD results. The solid lines represent least-squares fits to these values. The dashed line represents a linear extrapolation to $N^{-1/3}=0$. The extrapolated value $T_1/T_3=0.59$ is discussed in Sect. 3.1.

The size dependence of the T_1/T_3 and T_2/T_3 ratios for the present nanoparticles is summarized in Fig. 4. In this and in other plots of the current paper, the quantity $N^{-1/3}$ is used as an independent variable, because this quantity provides a measure of the surface/volume ratio, i.e., a characteristic that has long been used to systematize and explain the physical properties of nanoparticles[34–36]. Figure 4 indicates that the ratios T_1/T_3 and T_2/T_3 exhibit a similar rate of change with $N^{-1/3}$.

In closing this section we will discuss the value obtained by a linear extrapolation of the T_1/T_3 ratios to $N^{-1/3}=0$, which is represented by the dashed line in Fig. 4. To this aim we emphasize that the extrapolated temperature should strictly be interpreted as referring to a hypothetical state of macroscopic Au, with an atomic configuration similar to that of the SPL aggregates of the current nanoparticles. In line with this interpretation, the extrapolated ratio $T_1/T_3=0.59$ falls above 0.50, traditionally considered as the value of the T/T_f ratio above which diffusion processes become relevant in "actual" metallic solids with a melting temperature T_f[37].

3.2 The linear variation of MSD with T

The inset in Fig. 3 (b) indicates that below a certain temperature referred to as T^*, a linear variation of MSD with temperature is observed. For a macroscopic material, the possibility of a linear temperature dependence of the MSD might be understood, as a first approximation, by invoking the Debye model, which yields[32]:

$$(\delta_D\chi)^2=\frac{9\hbar^2T}{mk_B\theta_D^2} \quad (6)$$

In Eq.(6), $(\delta_D\chi)^2$ is the MSD due to the lattice vibrations, m is the atomic mass, θ_D is the Debye temperature, $\hbar$ and k_B the Planck and Boltzmann constants. However, there are at least two reasons why Eq.(6) should not be expected to account for the present results. In the first place, it is questionable to assume that the Debye model with the standard value of θ_D could describe the atomic vibrations under the anharmonic conditions plausibly holding in the current nanoparticles and temperatures approaching T^*. A second reason is that the current MD results indicate that surface diffusion, and to some extent, volume diffusion, contributes to the MSD in the high-temperature part of Region I. The discrepancy expected on the basis of these qualitative arguments is quantified in Table 1, where the values of $(\delta_D\chi)^2$ calculated at $T=T^*$ using Eq.(6) with the standard value θ_D= 165 K[38] are compared with the $(\delta_L\chi)^2$ from MD simulations. It is found that the actual MSD is, on the average, about 3.6 times that given by Eq.(6).

In view of the results in Table 1, it seems wise to refrain from adopting Eq.(6) to estimate the high-temperature properties of nanoparticles, as often done, e.g., when using the Debye-Lindemann melting formula at even higher temperatures[39–41].

Table 1 The MSD at the upper temperature boundary of the linear region (T^*) estimated by using Eq.(6) as $(\delta_D\chi)^2$, compared with that obtained from the MD simulated Lindemann ratios as $(\delta_L\chi)^2$ (Sect.3.1). The estimated uncertainties are follows: $\pm 25K$ in T^*, ± 0.002 Å^2 in $(\delta_D\chi)^2$, and ± 0.01 Å^2 in $(\delta_L\chi)^2$.

N	T^* (K)	$(\delta_D\chi)^2$ (Å^2)	$(\delta_L\chi)^2$ (Å^2)	$(\delta_L\chi)^2/(\delta_D\chi)^2$
1985	350	0.028	0.09	3.2
2491	325	0.026	0.10	3.8
2899	400	0.032	0.09	2.8
3151	325	0.026	0.09	3.5
3511	400	0.032	0.09	2.8
4537	350	0.028	0.11	3.9
5481	350	0.028	0.19	6.8
6699	400	0.032	0.11	3.4
11297	375	0.030	0.11	3.7
15707	450	0.036	0.12	3.3
25123	450	0.036	0.10	2.8
37215	450	0.036	0.10	2.8
84703	475	0.038	0.18	4.7

4 Discussion

4.1 Quasi-chemical modeling of the melting step

Building on early ideas of Berry and others[3,10,18–20], a thermodynamic model of the melting step (Region III) was proposed by the current authors[21], where HEA and LEA of Au coexist in a highly mixed state, such as that shown by the snapshots in Fig.3(b) of the current paper (and in Fig.2 of ref.[21]). The key assumption of the model is that in the melting step, atoms with the energy corresponding to the SPL boundary of the melting region (i.e., that located at T_2) and the HEA, with the energy corresponding to the LPL boundary of the melting step (i.e., that located at T_3) coexist in a dynamical equilibrium. Specifically, the model assumes that these two kinds of atoms, indicated as HEA-LPL and LEA-SPL respectively, are involved in the following isomerization-like chemical reaction:

View Article Online
DOI: 10.1039/D0CP04442C

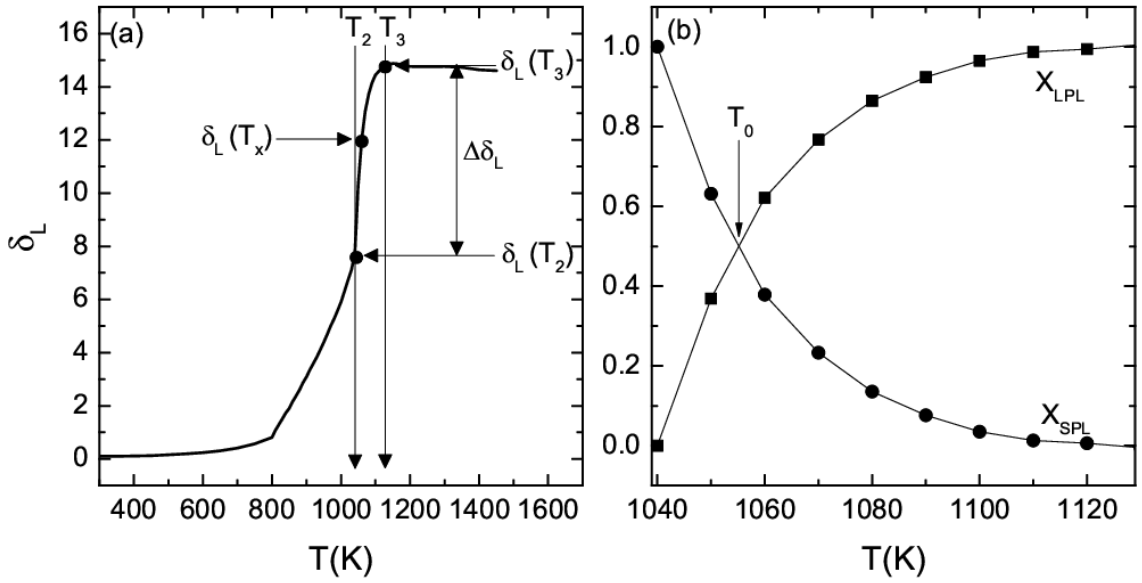

Fig. 5 (a) Scheme illustrating the determination of the quantities $\delta_L(T_2)$, $\delta_L(T_x)$, $\delta_L(T_3)$ and $\Delta\delta_L$ for the nanoparticle with 15707 atoms. (b) The temperature dependence of the quantities $X_{\text{HEA-LPL}}$ and $X_{\text{LHA-SPL}}$ estimated by using Eq.(11). The arrow indicates the temperature T_0 at which $X_{\text{LEA-SPL}} = X_{\text{HEA-LPL}}$, thus yielding (Eq.(8)) $K_{eq} = 1$ and $\Delta G = 0$.

$$\text{Au (LEA-SPL)} \rightleftharpoons \text{Au (HEA-LPL)} \tag{7}$$

Furthermore, in ref.[21] the classical equilibrium constant (K_{eq}) was introduced, which is related to the difference in Gibbs energy (ΔG) of Au between the SPL and LPL structures by the Van't Hoff relation

$$\Delta G = G^{\text{LPL}} - G^{\text{SPL}} = -RT \ln K_{eq} = -RT \ln \frac{X_{\text{HEA-LPL}}}{X_{\text{LEA-SPL}}} \tag{8}$$

In Eq.(8) the atomic fractions (X_j) usually adopted in macroscopic solution thermodynamics have been used to describe the relative amounts of HEA-LPL and LEA-SPL. By definition $X_{\text{HEA-LPL}} + X_{\text{LEA-SPL}} = 1$. In ref.[21] the $X_{\text{LEA-SPL}}$ and $X_{\text{HEA-LPL}}$ values were determined by describing the melting step part of the E versus T ("caloric curve") as the weighted sum of the contributions of the HEA-LPL and the LEA-SPL, as corresponds to an extensive thermodynamic property, viz.,

$$E(T_X) = (1 - X_{\text{HEA-LPL}})E(T_2) + X_{\text{HEA-LPL}}E(T_3) \tag{9}$$

where $T_2 < T_X < T_3$. From Eq.(9) one obtains the exact relation:

$$X_{\text{HEA-LPL}} = \frac{E(T_X) - E(T_2)}{E(T_3) - E(T_2)} \tag{10}$$

The evaluation of the various quantities in Eq.(10) from the "caloric curve" was explained in detail in Fig.6 of our previous work[21].

4.2 Evaluation of the T_0 temperature

By applying Eq.(10) to the melting step, Bertoldi et al.[21] determined the temperature dependence of the variables $X_{\text{LEA-SPL}}$ and $X_{\text{HEA-LPL}}$ for each nanoparticle, and used such information to determine the temperature at which $X_{\text{LEA-SPL}} = X_{\text{HEA-LPL}}$. At that temperature, called "the T_0 temperature", Eq.(8) yields $K_{eq} = 1$, and $\Delta G = 0$ i.e., the Gibbs energies of the Au atoms in the SPL and LPL states is the same. By this thermodynamic reason, T_0 might be considered as the nano-scale counterpart of the solid phase/liquid phase equilibrium temperature (T_f) in macroscopic Au.

In addition to using Eq.(10), a complementary, approximate procedure was used to estimate the $X_{\text{HEA-LPL}}$ values in the present work. The procedure is based on two empirical findings of the authors' work: (i) the quantities $E(T_3) - E(T_2)$ and $\delta_L(T_3) - \delta_L(T_2)$ are approximately proportional; and, (ii) the $\delta_L(T_3) - \delta_L(T_2)$ difference is approximately proportional to the number of atoms N of the nanoparticle. Both related findings allowed us to estimate $X_{\text{HEA-LPL}}$ (and $X_{\text{LEA-SPL}}$) by applying the following analogue of Eq.(10), where the ΔE differences are replaced by the well determined $\Delta\delta_L$ differences (Sect.3.1), viz.,

$$X_{\text{HEA-LPL}} \approx \frac{\delta_L(T_X) - \delta_L(T_2)}{\Delta\delta_L} \tag{11}$$

The evaluation of the various quantities in Eq.(11) from the information obtained in Sect.3.1 is explained in detail in Fig. 5(a), with reference to the nanoparticle with 15707 atoms. $\delta_L(T_X)$ is a general δ_L value in the melting step part of the δ_L versus T curve, viz. $\delta_L(T_2) \le \delta_L(T_X) \le \delta_L(T_3)$. The results of applying Eq.(11) to estimate the temperature dependence of the $X_{\text{HEA-LPL}}$ (and $X_{\text{LEA-SPL}}$) quantities, and therefrom the T_0 temperature (at which $X_{\text{LEA-SPL}} = X_{\text{HEA-LPL}}$), is described in Fig.5 (b).

View Article Online
DOI: 10.1039/D0CP04442C

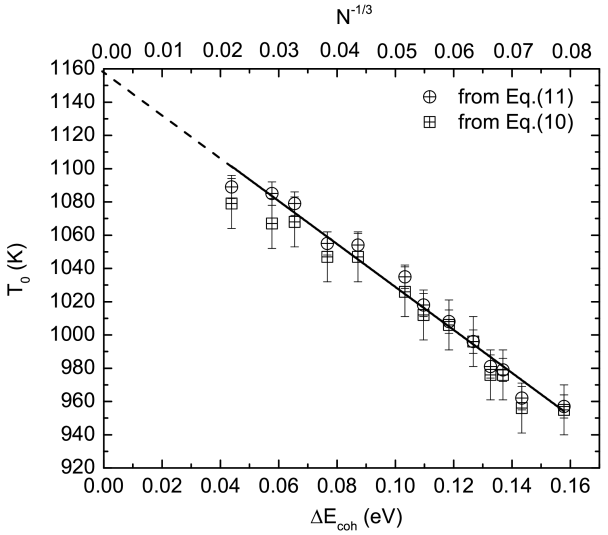

Fig. 6 Variation of the present T_0 temperature values (symbols) with $N^{-1/3}$ (upper scale) and with the cohesive energy difference ΔE_{coh} between macroscopic Au and each nanoparticle (lower scale) defined in Sect.2.3. Squares and circles represent the values obtained by applying Eq.(10) and Eq.(11), respectively, with the T_2 and T_3 temperatures determined in Sect.3.1. The solid line represents a least-squares fit to the results of Eq.(11). The dashed line describes a linear extrapolation to $N^{-1/3} = 0$, which yields $T_0 = 1158(\pm 6)$ K (see Sect. 4.2).

In Fig. 6, the T_0 values determined by applying Eqs. (10) and (11) using the temperatures T_2 and T_3 determined in Sect.3.1, agree well for most of the nanoparticles. In particular, the somewhat less scattered results given by Eq.(11) suggest a well-defined linear variation of T_0 with $N^{-1/3}$, and were given the highest weight in the remainder of this paper. The correlation in Fig.6 suggests that the variation of T_0 with $N^{-1/3}$ is due to the surface effect. In particular, the fact that the surface atoms are weakly bonded, is expected to correlate with the decrease in the average cohesive energy per atom of each nanoparticle with respect to the macroscopic material. This expectation is corroborated by the linear variation of T_0 with the quantity $\Delta E_{\text{coh}} = E^m_{\text{coh}} - E^{np}_{\text{coh}}$ (Sect.2.3) also represented in Fig. 6.

The results in Fig. 6 might be used to test the thermodynamically oriented interpretation of T_0 for nanoparticles as the counterpart of the temperature of fusion T_f of macroscopic Au. In the first place, a linear extrapolation to $N^{-1/3} = 0$ yields $T_0 = 1158(\pm 6)$K. The T_f temperatures obtained using EAM and similar extrapolations, viz., $1113(\pm 7)$K[21] and $1128(\pm 13)$K[29], and in previous Monte Carlo study of the macroscopic phases of Au yields 1090 K[42], i.e., comparable but somewhat lower values.. In the second place, the linear variation of T_0 with ΔE_{coh} and hence with the cohesive energy of the nanoparticles, is the analogue of the linear correlation between T_f and E_{coh}, which is usually accepted, on empirical grounds, for elemental solids[43].

4.3 Diffusion coefficients in the melting step

The thermodynamic and atomic configuration picture arrived at in the previous sections will be further developed by focusing on the kinetics of the process taking place in the melting step. To this aim, the diffusion coefficient (D) of the dynamic mixture of SPL-LEA and LPL-HEA was evaluated for each nanoparticle from the slope of the MSD versus time relation (Sect. 2.5)), as a function of temperature. The results are presented in Fig. 7 (a). A remarkable feature of these results is that D increases with temperature in the melting step, and reaches a maximum in the neighborhood of T_0. At even higher temperatures, D decreases (not shown in the figure). In the following, the maximum D values will be analyzed in order to illuminate their expected spatial dependence as well as their temperature dependence.

Concerning the spatial dependence, it is remarked that the maximum D values at $T = T_0$ (i.e., $D(T_0)$) increase with the radius of the particle, Fig. 7 (b), which suggests that larger nanoparticles offer more room for the atoms to move. Moreover, if the $D(T_0)$ values are correlated with $N^{-1/3}$, an essentially linear relation is obtained (not shown) although deviations are observed for the smallest sizes. Furthermore, a linear extrapolation to $N^{-1/3} = 0$ yields $D(T_0) = 0.164(\pm 0.006)$ Å^2/ps. This value will be compared with information for macroscopic Au obtained by the current authors by performing smooth extrapolations to T_0 of the D versus T values reported in the literature, as follows: (i) from the results of MD and Monte Carlo simulations, using a many-body potential based on the effective-medium theory, we estimate $D(1158\text{K}) \simeq 0.25$ Å^2/ps[44], (ii) from the results of MD simulations with LAMMPS using an EAM potential, we estimate $D(1158\text{K}) \simeq 0.18$ Å^2/ps[45] and, (iii) from the results of another MD simulations with an EAM potential, we estimate $D(1158\text{K}) \simeq 0.13$ Å^2/ps[46]. It is encouraging to find that the present $D(T_0)$ value agrees reasonably well with these numbers.

In turn, the temperature dependence of $D(T_0)$ is illustrated by the fact that the largest diffusion values correspond to the nanoparticles with the largest N, i.e., those with the highest T_0. In order to quantify in this feature, an attempt was made to evaluate the activation energy (E_A) for the diffusion processes at T_0. To this aim it was assumed that at this temperature the nanoparticles have essentially the same atomic configuration, since by definition, at T_0 the relative amounts of LEA-SPL and HEA-LPL is the same. On these basis, a $\ln(D(T_0))$ vs. $(1/k_B T_0)$ was constructed (Fig. 8). Except for the less precise values corresponding to the smallest four nanoparticles, which were therefore excluded from the fit, the data points are well represented by the straight solid line plotted in Fig. 8. Then, the Arrhenius-type relation

$$E_A = -\frac{\partial \ln D(T_0)}{\partial \left(\frac{1}{k_B T}\right)}, \tag{12}$$

allowed a reasonably accurate evaluation of an activation energy for in the current nanoparticles at T_0, viz., $E_A = (1.5 \pm 0.1)$ eV. This value is very close to the MD-EAM value $E_A = 1.68$ eV for self-diffusion in the solid phase of macroscopic Au[46]. Alternatively, from the already quoted D vs. T results for macroscopic Au, we estimate for the liquid phase $E_A \simeq 0.37$ eV (Ref.[44,46]) and $E_A \simeq 0.39$ eV (Ref.[45]), i.e., significantly smaller energies. These comparisons lend further support to the hypothesis that the diffusion properties at $T = T_0$ might be reasonably understood on

View Article Online
DOI: 10.1039/D0CP04442C

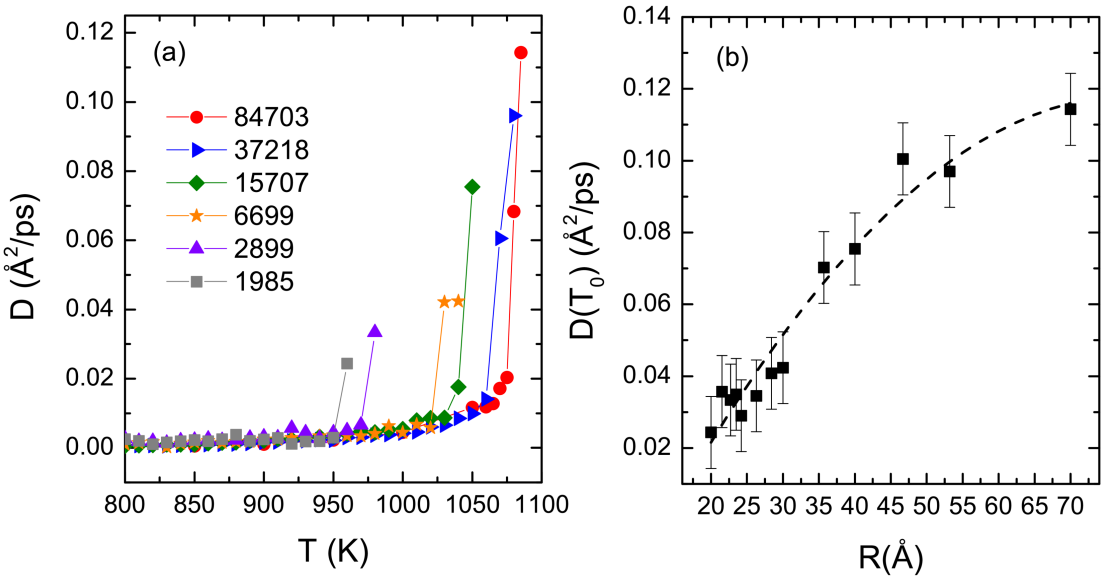

Fig. 7 (a) The diffusion coefficients (D) (symbols) versus temperature relations. (b) The maximum diffusion coefficients $D(T_0)$ occurring at the temperature T_0 (symbols) versus the radius (R) of the nanoparticles. In these plots, the solid or dashed lines are only guides to the eye.

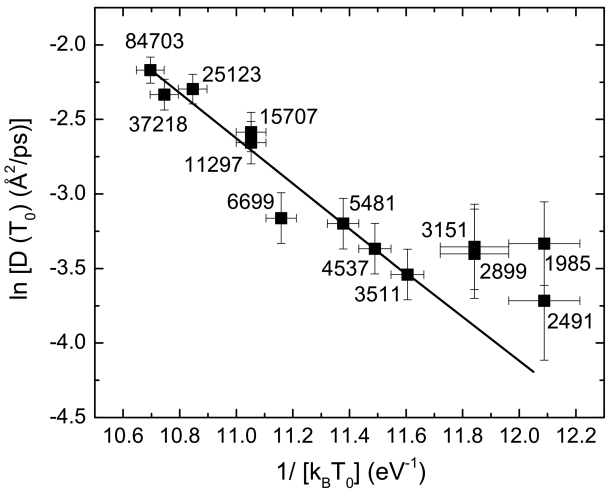

Fig. 8 The logarithm of the $D(T_0)$ diffusion coefficients (symbols with error bars) versus the inverse of the product of the T_0 temperature and Boltzmann's constant k_B. The solid line represents the least-squares fit to all but the four smallest particles results. By applying Eq.(12) an energy corresponding to the activation of the atomic movements in the current nanoparticles at T_0, viz., $E_A = 1.5(\pm 0.1)$ eV, was evaluated.

the basis of the existence of a dynamic mixture of LEA-SPL and HEA-LPL. Specifically, the advance of the melting process requires movements of the LEA-SPL, i.e., those expected to require the largest activation energy. In line with such picture, the current results indicate that the energy necessary to activate the LEA-SPL is close to that predicted by MD-EAM for the diffusion in solid macroscopic Au.

In summary, the current $D(T_0)$ values describe the diffusion processes in a series of nanoparticles formed by equi-atomic mixtures of LEA and HEA. Consequently, these values show the spatial and temperature dependences of the diffusion coefficients one could expect when treating a set of nano-systems of the same element and essentially the same atomic configuration (or "structure") namely, an increase with the size of the system and with temperature, but the same activation energy.

5 Summary and concluding remarks

The present paper builds on a previous thermodynamic and structural analysis of the heating and melting of Au nanoparticles by the current authors, based on MD results on the temperature dependence of the energy, the Lindemann index, as well as the root-mean square displacement and the radial distribution function[21].

The specific aim of the present work was to gain understanding on the interrelations between the atomic configuration, and the thermodynamic and kinetic features of the change, induced by heating, from the solid-phase like (SPL) to the liquid-phase like (LPL).

In order to access theoretically such interrelations, the current MD-EAM simulations made use of the temperature dependence of the mean-square displacement (MSD) and the Lindemann ratio. In this way, a four-step phenomenological model of the changes in atomic confirmation upon heating was developed, and the temperature (T) boundaries of the various regions were determined and systematized as a function of the size of the nanoparticles. Two such regions were then analyzed in greater detail. One region, located in the low temperature part of the studied range, is characterized by a linear variation of the MSD with T. The other region, called the "melting step", occurring in the high temperature part of the range, is characterized by rapid variations of the MSD with T.

The latter region was treated in terms of a physico-chemical model hypothesizing the existence of two kinds of Au atoms, coexisting in dynamical thermodynamic equilibrium, viz., low-

View Article Online
DOI: 10.1039/D0CP04442C

energy atoms (LEA) with an energy corresponding to the low-T boundary (i.e., the SPL boundary) of the melting step in the caloric curve, and high-energy atoms (HEA) with an energy corresponding to the high-T boundary (i.e., the LPL boundary) of the "melting step" in the caloric curve.

The classical equilibrium constant describing the isomerization-like reaction Au (LEA-SPL) $\rightleftharpoons$ Au (HEA-LPL) was introduced, and the atomic fractions of the LEA-SPL and HEA-LPL were determined as a function of T. These fractions were used to evaluate the equal-Gibbs energy temperature ("T_0 temperature") which is the thermodynamic counterpart of the solid phase/liquid phase equilibrium temperature of macroscopic Au. The size dependence of T_0 was discussed.

Moreover, the kinetic properties of the "melting step" mixture of LEA-SPL and HEA-LPL were investigated by focusing on the diffusion coefficient (D) which shows a local maximum at $T \simeq T_0$. It is found that the $D(T_0)$ values increase with the size of the nanoparticles, and with the value of T_0. These spatial and temperature dependences of $D(T_0)$ were rationalized by considering that, by definition of T_0, the various nanoparticles involve equal atomic fractions of LEA-SPL and HEA-LPL, that is, they have essentially the same atomic configuration (or "structure").

An Arrhenius-type analysis of the $\ln(D(T_0))$ vs. $(1/k_B T_0)$ plot yields a well-defined activation energy for the atom movements that is remarkably close to that determined by previous MD-EAM simulations on solid macroscopic Au. Such an agreement lends support to a direct implication of the current picture of the "melting step", viz., the progress upon heating of the SPL-to-LPL change needs the activation of the LEA-SPL, i.e., those requiring the largest activation energy.

Acknowledgements

This work has been supported by Consejo Nacional de Investigaciones Científicas y Técnicas (CONICET, Argentina) under Project PIP 11220170100761CO.

Notes and references

1 J. Jellinek, T. L. Beck and R. S. Berry, *The Journal of Chemical Physics*, 1986, **84**, 2783–2794.
2 T. L. Beck and R. S. Berry, *The Journal of Chemical Physics*, 1988, **88**, 3910–3922.
3 R. S. Berry, *Scientific American*, 1990, **263**, 68–75.
4 C. L. Cleveland, W. D. Luedtke and U. Landman, *Physical Review B*, 1999, **60**, 5065–5077.
5 J.-H. Shim, B.-J. Lee and Y. W. Cho, *Surface Science*, 2002, **512**, 262–268.
6 Y. Wang, S. Teitel and C. Dellago, *Chemical Physics Letters*, 2004, **394**, 257–261.
7 W. Hu, S. Xiao, J. Yang and Z. Zhang, *The European Physical Journal B*, 2005, **45**, 547–554.
8 F. Baletto and R. Ferrando, *Reviews of Modern Physics*, 2005, **77**, 371.
9 H. Duan, F. Ding, A. Rosén, A. R. Harutyunyan, S. Curtarolo and K. Bolton, *Chemical Physics*, 2007, **333**, 57–62.
10 R. S. Berry and B. M. Smirnov, *Chemical Physics Letters*, 2013, **573**, 1–4.
11 G. Guenther and O. Guillon, *Journal of Materials Science*, 2014, **49**, 7915–7932.
12 Z. Qiao, H. Feng and J. Zhou, *Phase Transitions*, 2014, **87**, 59–70.
13 I. Hamid, M. Fang and H. Duan, *AIP Advances*, 2015, **5**, 047129.
14 H. Li, R. Xu, Z. Bi, X. Shen and K. Han, *Journal of Electronic Materials*, 2017, **46**, 3826–3830.
15 T. Li, C. He, W. Zhang and M. Cheng, *Journal of Alloys and Compounds*, 2018, **752**, 76–84.
16 X. Zhang, W. Li, D. Wu, Y. Deng, J. Shao, L. Chen and D. Fang, *Journal of Physics: Condensed Matter*, 2018, **31**, 075701.
17 M. Kateb, M. Azadeh, P. Marashi and S. Ingvarsson, *Journal of Nanoparticle Research*, 2018, **20**, 251.
18 R. S. Berry and B. M. Smirnov, *The Journal of Chemical Physics*, 2001, **114**, 6816–6823.
19 R. S. Berry and B. M. Smirnov, *International Journal of Mass Spectrometry*, 2009, **280**, 204–208.
20 J. D. Honeycutt and H. C. Andersen, *Journal of Physical Chemistry*, 1987, **91**, 4950–4963.
21 D. S. Bertoldi, E. N. Millán and A. F. Guillermet, *Journal of Physics and Chemistry of Solids*, 2017, **111**, 286–293.
22 T. P. Duy and V. V. Hoang, *Physica B: Condensed Matter*, 2012, **407**, 978–984.
23 L. V. Sang, V. V. Hoang and D. T. N. Tranh, *The European Physical Journal D*, 2015, **69**, year.
24 Z. H. Jin, P. Gumbsch, K. Lu and E. Ma, *Physical Review Letters*, 2001, **87**, year.
25 S. Plimpton, *Journal of Computational Physics*, 1995, **117**, 1–19.
26 S. M. Foiles, M. I. Baskes and M. S. Daw, *Physical Review B*, 1986, **33**, 7983–7991.
27 S. Ali, V. S. Myasnichenko and E. C. Neyts, *Physical Chemistry Chemical Physics*, 2016, **18**, 792–800.
28 Y. G. Chushak and L. S. Bartell, *The Journal of Physical Chemistry B*, 2001, **105**, 11605–11614.
29 L. J. Lewis, P. Jensen and J.-L. Barrat, *Physical Review B*, 1997, **56**, 2248–2257.
30 R. Essajai, A. Rachadi, E. Feddi and N. Hassanain, *Materials Chemistry and Physics*, 2018, **218**, 116–121.
31 A. Prakash, M. Hummel, S. Schmauder and E. Bitzek, *MethodsX*, 2016, **3**, 219–230.
32 G. Grimvall, *Thermophysical properties of materials*, Elsevier, Amsterdam, Netherlands New York, 1999.
33 Y. Wang, S. Teitel and C. Dellago, *The Journal of Chemical Physics*, 2005, **122**, 214722.
34 H. Li, R. Xu, Z. Bi, X. Shen and K. Han, *Journal of Electronic Materials*, 2016, **46**, 3826–3830.
35 S. Krüger, S. Vent and N. Rösch, *Berichte der Bunsengesellschaft für physikalische Chemie*, 1997, **101**, 1640–1643.
36 G. Guenther and O. Guillon, *Journal of Materials Science*,

View Article Online
DOI: 10.1039/D0CP04442C

2014, **49**, 7915–7932.
37 B. Cox, *MG Fontana and RW Staehle, eds*, 1976, **5**, 173.
38 C. Kittel, *Introduction to Solid State Physics. Fifth edition*, 1976.
39 Q. Jiang, H. Tong, D. Hsu, K. Okuyama and F. Shi, *Thin Solid Films*, 1998, **312**, 357–361.
40 Y. F. Zhu, J. S. Lian and Q. Jiang, *The Journal of Physical Chemistry C*, 2009, **113**, 16896–16900.
41 J. Chandra and K. Kholiya, *Modern Physics Letters B*, 2015, **29**, 1550025.
42 S. M. Foiles and J. B. Adams, *Physical Review B*, 1989, **40**, 5909–5915.
43 G. Grimvall and S. Sjödin, *Physica Scripta*, 1974, **10**, 340–352.
44 A. Bogicevic, L. B. Hansen and B. I. Lundqvist, *Physical Review E*, 1997, **55**, 5535.
45 H. Sheng, *EAM potentials*, `https://sites.google.com/site/eampotentials/Au`.
46 J. Akhter, E. Ahmed and M. Ahmad, *Materials Chemistry and Physics*, 2005, **93**, 504–507.